



HAL
open science

Sr 1/2 Ce 5/14 1/7 WO 4; a new modulated ternary scheelite compound

Rafael Hernandez Damascena dos Passos, Madjid Arab, Carlson Pereira de Souza, Christine Leroux

► **To cite this version:**

Rafael Hernandez Damascena dos Passos, Madjid Arab, Carlson Pereira de Souza, Christine Leroux. Sr 1/2 Ce 5/14 1/7 WO 4; a new modulated ternary scheelite compound. Acta Crystallographica Section B: Structural Science, Crystal Engineering and Materials [2014-..], 2017, 73 (3), pp.466 - 473. 10.1107/S2052520617002827 . hal-01824375

HAL Id: hal-01824375

<https://univ-tln.hal.science/hal-01824375>

Submitted on 27 Jun 2018

HAL is a multi-disciplinary open access archive for the deposit and dissemination of scientific research documents, whether they are published or not. The documents may come from teaching and research institutions in France or abroad, or from public or private research centers.

L'archive ouverte pluridisciplinaire **HAL**, est destinée au dépôt et à la diffusion de documents scientifiques de niveau recherche, publiés ou non, émanant des établissements d'enseignement et de recherche français ou étrangers, des laboratoires publics ou privés.

$\text{Sr}_{1/2}\text{Ce}_{5/14}\square_{1/7}\text{WO}_4$; a new modulated ternary scheelite compound

Rafaël Hernandez Damasceno dos Passos,^{a,b} Madjid Arab,^a Carlson Pereira De Souza,^b and Christine Leroux^{a,*}

^a Université de Toulon, CNRS, IM2NP, BP 20132, F- 83957 La Garde Cedex, France

^b Universidade do Rio Grande de Norte, DEQ/PPGEQ-LMNRC, Campus Universitario, Lagoa Nova 59072-970 Natal, Brazil

Correspondence e-mail: leroux@univ-tln.fr

Synopsis - A new ternary scheelite tungstate $(\text{Sr,Ce})\text{WO}_4$ phase was synthesized, with a 2D incommensurately modulated structure linked to partial ordering of Sr, Ce cations and vacancies as was evidenced by high resolution electron microscopy. The band gap of 3.2 eV makes it a promising violet emitting compound.

Abstract - type the Abstract here (Style: IUCr Abstract)

For the first time, a ternary tetragonal scheelite tungstate with strontium and cerium cations, $(\text{Sr,Ce})\text{WO}_4$, was synthesized. As much as 35 % Ce could be inserted in the structure, leaving 1/7 of the (Sr,Ce) cation sites vacant. Partial ordering of Sr and Ce, with atomic displacements, were evidenced by high resolution electron microscopy. 2D incommensurate modulations occur in this material, in small domains 20 nm in size. The band gap of this compound is significantly lower than the band gap of SrWO_4 and this was related to the distortions of WO_4 and $(\text{Sr,Ce})\text{O}_8$ polyhedra. The band gap value of 3.2 eV makes $\text{Sr}_{1/2}\text{Ce}_{5/14}\square_{1/7}\text{WO}_4$ a promising candidate for violet luminescence.

Keywords: - scheelite, ordering, vacancies, incommensurate, high resolution electron microscopy, simulations, x ray diffraction, band gap.

1. Introduction

Scheelite molybdates or tungstates are known to be chemically stable luminescent compounds as well as good ionic conductors. In the last decade, their potential use as light emitting materials was explored and many new scheelite compounds were synthesized, by adding lanthanide cations in the structure (Abakumov *et al.*, 2014; Morozov *et al.*, 2013, Nogueira *et al.*, 2013, Giang *et al.*, 2015). The binary scheelite tetragonal structure of general formula ABO_4 , (space group $I4_1/a$) corresponds to $(\text{A}^{2+}, \text{B}^{6+})$ and the cation/anion ratio $[\text{A}]/[\text{BO}_4]$ is equal to 1. The structure, shown Fig.1, can be described as a piling up of layers along

the c axis built by $[\text{BO}_4]$ tetrahedra and $[\text{AO}_8]$ polyhedra sharing vertices. This structure accommodates easily cations with different oxidation states for A and B as in BiVO_4 ($\text{A}^{3+}, \text{B}^{5+}$), ZrGeO_4 ($\text{A}^{4+}, \text{B}^{4+}$) or AgIO_4 ($\text{A}^+, \text{B}^{7+}$). When the cation/anion ratio is different from 1, the tetragonal structure of binary tungstate ($\text{B}=\text{W}$) or molybdate ($\text{B}=\text{Mo}$) scheelite can be distorted into a monoclinic structure as in $\text{Ce}_2\text{W}_3\text{O}_{12}$ ($\text{A}^{3+}, \text{B}^{6+}$) (Arab *et al.*, 2013) or an orthorhombic one as in $\text{Ce}_{10}\text{W}_{22}\text{O}_{81}$ (Patout *et al.*, 2014). Ternary scheelites refer to compounds with general formula $(\text{A}, \text{A}')_n(\text{BO}_4)_m$. Most of them are built with a charge difference of 2 between A et A' cations, as for example $(\text{Ag}, \text{RE})(\text{MoO}_4)_2$ or $(\text{Li}, \text{RE})(\text{MoO}_4)_2$ RE=rare earth elements (Abakumov *et al.*, 2014). The charge difference is usually accommodated by cation vacancies on A sites, with or without cation ordering or incommensurate modulations (Abakumov *et al.*, 2014). Ternary scheelite with a charge difference of 1 are uncommon, and apart from a lead-lanthanide based compound (Takai *et al.*, 2004), only $(\text{Ca}, \text{Eu})(\text{BO}_4)_2$ and $(\text{Sr}, \text{Eu})(\text{BO}_4)_2$ were extensively studied (Abakumov *et al.*, 2014; Jiang *et al.*, 2015).

Among rare earth compounds with the scheelite structure, rare earth tungstates exhibit excellent thermal and chemical stability. Tungstates have been proven to be good host lattices for the luminescence of lanthanide ions (Zhou *et al.*, 2014). Eu^{3+} is a commonly used luminescent activator and Eu^{3+} activated SrWO_4 are efficient light emitting diodes (LED) (Jiang *et al.*, 2015). An interesting alternative to Eu^{3+} is Ce^{3+} because of a potential tunable light emission. The light emission of Ce^{3+} varies from ultraviolet to orange, depending on the crystal field (Zhu *et al.*, 2016; Li *et al.*, 2008). The mechanism of Ce light emission is usually linked to the interaction of the incomplete 4f shell energy levels of Ce with the band state of the host lattice (E. Roy *et al.*, 2010). The determination of the band gap is one way to obtain information of the potential optical properties of one compound. As the band gap value is also linked to the structural defects around the lanthanide ions, which are promoted by the distortions of angles and bond distances within different polyhedra clusters, (Cavalcante *et al.*, 2012; Rosa *et al.*, 2008; Lacomba-Perales *et al.*, 2008), structural investigations have to be linked to optical characterizations.

The aim of this work was to synthesize a $(\text{Sr}, \text{Ce})\text{WO}_4$ ternary scheelite compound with different optical properties compared to those of the binary scheelite SrWO_4 . A complexing method was used to synthesize powders of binary SrWO_4 , and $(\text{Sr}, \text{Ce})\text{WO}_4$ ternary tungstate scheelites. Rietveld refinements of the X ray diffraction patterns were performed to obtain accurate cell parameters and atomic distances. Electron diffraction and high resolution electron microscopy gave access to the incommensurate modulations and cation ordering. The chemical composition was determined by Energy Dispersive Spectroscopy (EDS) and the

cation valence by Electron Energy Loss Spectroscopy (EELS). UV-Visible Diffuse Reflectance Spectra (DRS) was used to determine the energy band gap.

We showed that the $(\text{Sr,Ce})\text{WO}_4$ has an incommensurate modulated structure linked to partial ordering of Sr^{2+} and Ce^{3+} . The influence of the structure on the band gap values was discussed in terms of bonds distances and angles splitting of the polyhedra WO_4 and $\text{Sr}(\text{Ce})\text{O}_8$.

2. Experimental procedures

2.1. Synthesis

The powders were synthesized by the so called EDTA-citrate complexing method, EDTA accounting for Ethylene-Diamine-Tetracetic-Acid. This method was already used to obtain binary tungstates SrWO_4 and $\text{Ce}_2\text{W}_3\text{O}_{12}$, (Arab *et al.*, 2013) and was adapted in this work to synthesize ternary tungstates. Strontium nitrate $\text{Sr}(\text{NO}_3)_2$, cerium(III) nitrate hexahydrate $\text{Ce}(\text{NO}_3)_3 \cdot 6\text{H}_2\text{O}$ and tungsten oxide WO_3 were used as cation source. EDTA was diluted in ammonium hydroxide (27% vol.) NH_4OH at 40°C with a constant stirring during 15 min. Solutions 0.3 M of strontium and cerium nitrates and WO_3 were added in the solution of the EDTA/ NH_4OH in various proportions and stirred 15 minutes again. Then 0.45 M citric acid was added to initiate the complexation reaction at a temperature of 80°C and at $\text{pH} = 9$. The reaction time lasted 3h until the appearance of a gel-like precipitate. This gel was subjected to a heat pretreatment at a temperature of 230°C for 3h to remove waste liquids and volatiles, leading to the formation of a black powder. The final annealing was performed at 1000°C for 5h, a temperature ensuring the crystallization of the gel, leading to yellowish-white powders.

2.2. Structural and chemical characterization

Transmission Electron Microscopy (TEM) and High Resolution Electron Microscopy (HREM) were performed with a conventional Tecnai 200 kV and with a Titan FEG 300 kV C_s corrected, equipped with a Gatan Imaging Filter (GIF). Simulated HREM images were calculated using the multislice program JEMS. The parameters used for simulations of images taken with the 300 kV microscope were $C_s = -1.9\mu\text{m}$, $C_c = 2\text{ mm}$, $1/2 \alpha = 1\text{ mrad}$, $\Delta E = 0.7\text{ eV}$. The chemical composition of the ternary tungstate was determined by Energy Dispersive spectroscopy (EDS). Binary compounds SrWO_4 and $\text{Ce}_2\text{W}_3\text{O}_{12}$ were used as standards for the determination of the $K_{\text{Sr,W}}$ and $K_{\text{Ce,W}}$ factors. The statistical study of powder's chemical homogeneity consisted in 20 EDS analyses on randomly chosen individual grains. Electron Energy Loss Spectroscopy (EELS) gave access to the valence of cerium in the ternary compound. Spectra were acquired in the diffraction mode, with a 0.03 eV/channel resolution. X rays powder diffraction (XRD) patterns were collected in the classical $\theta-2\theta$ mode, with an Empyrean Panalytical diffractometer, with a Cu anti cathode ($\lambda_{\text{K}\alpha 1} = 0.154056\text{ nm}$), Rietveld

refinements with the software Fullprof were performed, starting from data cif files found in literature, and cell parameters, atomic positions, as well as site occupations, were extracted. The experimental profiles were fitted with the most suitable pseudo-Voigt analytical function taking into account the line broadening function and the symmetric part of instrumental function.

2.3. Optical properties

The band gap values were obtained using the UV-visible diffuse reflectance spectroscopy (DRS). The spectra of the different samples were recorded using a Perkin Elmer LAMBDA 190s UV/Vis/NIR spectrometer along with a 150 mm integrating sphere. A given powder was compacted in a manual press into a 1.2 cm powder cup, clamped on the external port of the integrating sphere. The measurements were performed in the range of 250 to 800 nm at room temperature with a resolution of 0.08 nm. The baseline was determined using a calibrated reflectance standard to allow achievement of a reflectance accuracy of 0.5%.

3. Results

3.1. Chemical composition

The mean composition of the ternary compound was found to be $\text{Sr}_{0.50}\text{Ce}_{0.35}\text{WO}_4$, which can also be written $\text{Sr}_{1/2}\text{Ce}_{5/14}\square_{1/7}\text{WO}_4$, emphasizing the occurrence of cation vacancies. Although the majority of ternary tungstate or molybdate are stoichiometric, ternary scheelite compounds with cations vacancies were already mentioned (Abakumov *et al.*, 2014). Ce^{3+} may partially oxidized into Ce^{4+} , thus the valence state of cerium in $\text{Sr}_{0.50}\text{Ce}_{0.35}\text{WO}_4$ was determined by EELS. Ce^{4+} and Ce^{3+} $M_{4,5}$ core loss edges can unambiguously be distinguished due to differences in shape, intensities and energies (Garvie *et al.*, 1999). The Ce^{4+} $M_{4,5}$ edges consist in two main symmetrical peaks situated at 884 eV and 901.6 eV and two satellites peaks of lower intensities at 889.2 eV and 906.7 eV. On the contrary, the Ce^{3+} M_4 edge is asymmetrical with features at 896.6, 898.4 and 899.7 eV and the Ce^{3+} M_5 edge shows a broad maximum from 881.7 to 882.3 eV. Apart from the shape and energy positions of the energy loss peaks, the branching ratio, defined as the intensity ratio $I(M_5)/[I(M_4)+I(M_5)]$, can be used to distinguish between Ce^{3+} (branching ratio 0.55) and Ce^{4+} (branching ratio 0.49). Fig. 2 shows a characteristic EELS spectrum, acquired on a single grain of the ternary powder. The best fit was obtained with two peaks at 882 and 883 eV for the M_5 edge and three peaks at respectively 896.9, 898.5 and 899.8 eV for the M_4 edge, indicating the cerium is in a 3+ valence state in the ternary scheelite compound. However, the occurrence of two peaks

around 883 eV, and a branching ratio of 0.53, indicate the presence of Ce^{4+} . Assuming the linear relation between branching ratio and relative amount of Ce^{4+} proposed by Gravier et al. (1999), one can estimate the Ce^{4+} amount to be around 30%.

3.2. Electron diffraction

The main spots of the electron diffraction (ED) pattern, taken under different zone axes, could all be indexed in the tetragonal scheelite structure. Fig.3 presents high symmetry ED patterns, with respectively [001], [100], [1-10] and [111] zones axes, indexed in the tetragonal structure. In the ED pattern taken along [001] (Fig.3a), the main spots exhibit the characteristic four fold symmetry of the tetragonal structure along c, but the weaker spots cannot be indexed with integer indices. They correspond to two incommensurate vectors, $\mathbf{q}_1=0.54 \mathbf{a}^*+0.82 \mathbf{b}^*$, $\mathbf{q}_2= -0.82 \mathbf{a}^*+0.54 \mathbf{b}^*$, thus to a two dimensional structure modulation, which led to an indexation of the different ED patterns in a (3+2)D superspace group with 5 indices (Van Smaalen *et al.*, 2007). Spots, indexed (00l00) with $l=2n$, that are forbidden in the space group $I4_1/a$ of the tetragonal scheelite structure, can be observed in Fig 3b and 3c. During tilt experiments, these spots do not vanish, excluding a double diffraction phenomenon. A reduction in symmetry must then be considered from $I4_1/a$ to $I-4$ (82). This symmetry loss was already observed for ternary scheelite molybdate like $(\text{Na,Gd})\text{MoO}_4$ (Abakumov *et al.*, 2012) or $(\text{Li,Yb})\text{MoO}_4$ (Volkov *et al.*, 2005). Thus, the superspace group for $\text{Sr}_{0.50}\text{Ce}_{0.35}\text{WO}_4$ was identified as $I-4$ ($\alpha,\beta,0, -\beta\alpha 0$)00, with $\alpha= 0.54$ and $\beta=0.82$. Fig.4 is part of the [001] pattern, where the two incommensurate vectors \mathbf{q}_1 and \mathbf{q}_2 are drawn: all the weak spots in the ED pattern can be indexed using \mathbf{q}_1 and \mathbf{q}_2 . Modulated structures are not uncommon in $(\text{A,A}')_n(\text{BO}_4)_m$ scheelite compounds (B=Mo or W) and an exhaustive overview of them can be found in (Abakumov *et al.*, 2014). This overview was realized in order to study the origin of these modulations, which were linked to the difference in cation sizes, the ordering of the A, A' cations and the presence of cations vacancies in the A sublattice. With a radius difference of $\Delta r=0.1 \text{ \AA}$ between Sr^{2+} and Ce^{3+} , and 1/7 of vacancies, $\text{Sr}_{1/2}\text{Ce}_{5/14}\square_{1/7}\text{WO}_4$ belongs to the same group of partially ordered scheelites as $\text{Na}_{2/7}\text{Gd}_{4/7}\square_{1/7}\text{MoO}_4$ (Abakumov *et al.*, 2012). The same modulations vectors $\mathbf{q}_1=0.54 \mathbf{a}^*+0.82 \mathbf{b}^*$, $\mathbf{q}_2= -0.82 \mathbf{a}^*+0.54 \mathbf{b}^*$ are observed for these structures, but the charge difference Δq between A and A' cations is $\Delta q =2$ ($\text{Na}^+, \text{Gd}^{3+}$) in one case, $\Delta q=1$ in the other one ($\text{Sr}^{2+}, \text{Ce}^{3+}$). Another difference is that two-dimensional incommensurate modulations were observed in molybdates with tetragonal structure but not in tungstate scheelites. On the contrary, ternary tungstate scheelites usually adopt a (3+1) D modulated monoclinic structure (Morozov *et al.*, 2013). Thus, one can conclude that 2D modulations are linked to a small Δr and vacancies on A sites, but not to Δq , the charge difference between A and A' cations. Moreover, these modulations can occur in tungstates, not only in molybdates.

3.3. High resolution electron microscopy

High resolution electron microscopy (HREM) observations were performed along the [001] direction, where the projected structure corresponds to mixed columns of Sr, Ce and W cations, (see Fig5a) and along [111], where the projected structure corresponds to distinct atomic columns for the (Sr,Ce) cations and for W (Fig 5b).

Fig6 shows a HREM image taken along [001], along with a Fast Fourier Transform (FFT) and filtered images. The FFT image is similar to the diffraction pattern Fig4, with the same incommensurate spots. FFT performed on different regions of the HREM image do not always exhibit these spots, which indicate that modulations are localised in domains. The filtered image using the incommensurate spots confirms a 10-20 nm domain-type structure. The filtered image, using Bragg spots 20000 and 02000, has an enhanced contrast compared to the original image, shows no defects and can be interpreted in terms of atomic columns of cations.

In order to study a possible ordering of Sr and Ce, HREM images were taken along [111], using a 300 KV microscope Cs corrected. This projection direction allows to interpret HREM images in terms of atomic columns of W, Sr, Ce (Fig5.b). In particular, along the trace of (112) planes, there will be successively two W columns, two (Sr,Ce) columns. Fig.7 shows a HREM image taken along [111] where thickness variations give rise to different motifs. The two insets correspond to filtered images from a thin part and a thick part of the sample. In the thin part of the sample, the position of the bright spots as well as their intensity clearly varies along the trace of the (112) planes, suggesting different atomic occupation. Simulated HREM images were calculated using two structural models and compared to the filtered images. Both structural models were based on the I-4 space group deduced from the ED study. The first model (model 1) corresponds to a disordered scheelite structure; Sr, Ce cations occupy randomly the same 2(b) and 2(c) sites, and W is on the 2(a) and 2(d) sites. This structural model was already used for $\text{Na}_{2.7}\text{Gd}_{4.7}\text{MoO}_4$ (Morozov *et al.*, 2012). In the second model (model 2), the Sr cations occupy the 2(b) site while the Ce cations are on 2(c) sites. The chemical composition was taken into account, thus vacancies were statistically distributed on 2(b) and 2(c) sites for both models. The atomic positions are summarized in Table 1.

The pattern observed in the thick part of the sample can solely be simulated with the structural model where Ce and Sr are ordered, for a thickness of 5-7 nm (Fig.8). The pattern observed in the thin part can, at first sight, be simulated for both disordered and ordered model, but the intensity variation observed along one row corresponds strictly to the different site occupation for strontium and cerium, as can be seen in Fig.8 where the projected structure is superimposed to a simulated one for a weak thickness of 3 nm. Thus, HREM allowed to prove experimentally the ordering of strontium and cerium atoms in $\text{Sr}_{0.50}\text{Ce}_{0.35}\text{WO}_4$.

3.4. Crystal structure refinements (X ray diffraction)

Fig.9 reports the XRD patterns of the binary SrWO_4 (Fig.9a) and of the new ternary $\text{Sr}_{0.50}\text{Ce}_{0.35}\text{WO}_4$ (Fig.9b) compounds. The diagrams correspond to well crystallized single phases without residual compounds. The phase identification showed that both tungstates exhibit XRD diagrams characteristic of the tetragonal scheelite structure. In particular, the splitting of the high angle peaks induced by a monoclinic structure, was not observed.

We performed different Rietveld refinements of the XRD patterns, according to electron microscopy results. The binary compound SrWO_4 was refined in the $I4_1/a$ space group. The ternary compound $\text{Sr}_{0.50}\text{Ce}_{0.35}\text{WO}_4$ was refined in the $I4_1/a$ space group and in the $I-4$ space group, with a random occupation of A sites by Ce^{3+} and Sr^{2+} (the so called disordered scheelite). The occupation rate of the A sites was fixed to 50% for Sr and 35% for Ce, according to EDS results. In both space groups, the cations occupy fixed Wyckoff positions (see Table 1) and only the coordinates of oxygen atoms were refined. The refinements were initiated using cif files already published (Pereira *et al.*, 2015; Abakumov *et al.*, 2012). The refined cell parameters, oxygen coordinates and reliability factors are reported in Table 2.

The refinements in the $I4_1/a$ space group provides a good agreement with the experimental data for the binary and the ternary compounds, with acceptable reliability factors. The cell parameters of the ternary scheelite $\text{Sr}_{0.50}\text{Ce}_{0.35}\text{WO}_4$ are smaller than those of the binary SrWO_4 , with a shrinkage of the unit cell of about 1,4% in volume. This is in agreement with the substitution of Sr^{2+} by Ce^{3+} , which has a smaller radius ($\Delta r = -0.1 \text{ \AA}$) and the induced cation vacancies. The loss of symmetry from the $I4_1/a$ space group to the $I-4$ one, corresponds to a splitting of each atomic position (see Table 1). Thus, the cations were distributed on the different sites according to model 1 (no ordering of Sr and Ce). Again, the reliability factors show a good agreement between the calculated and the experimental diffraction patterns. The differences in the reliability factors for the two refinements of the $\text{Sr}_{0.50}\text{Ce}_{0.35}\text{WO}_4$ structure are too small to discriminate between the two possible space groups ($N^\circ 82$ and 88). This can be related to the polycrystalline character of our samples with heterogeneous size distribution in the nanometer range. Thus, investigations of a possible cation ordering through Rietveld refinements of XRD diagrams were meaningless.

The variation in the atomic coordinates observed for oxygen atoms, gives rise to different distortions of the polyhedra as can be seen in Table 3, which summarizes the A–O and W–O bond lengths and angles. The cerium insertion in the SrWO_4 scheelite structure leads to a contraction of WO_4 tetrahedra and an expansion of AO_8 polyhedra.

Basically, the SrWO_4 binary compound presents a main W–O distance of $1,8408 \text{ \AA}$ and two characteristic O–W–O angles values of 107° and 114° . The W–O distance decreases to 1.7903 \AA in the $\text{Sr}_{0.50}\text{Ce}_{0.35}\text{WO}_4$ structure with $I4_1/a$ space group, but the O–W–O angles

remain the same, 107.7° and 113°. The A-O bond length increases, showing the WO₄ contraction is accompanied by a AO₈ expansion, and the O-A-O angles do not change significantly. On the contrary, the refined structure with the I-4 space group shows much more WO₄ and AO₈ distortions. In this space group there are two W-O distances of 1.7964 and 1.7554 Å. The O-W-O angles deviate much more from the ideal tetrahedral angle of 109.9°, with values of 104°, 105°, 111°, 120° respectively. Similarly, the AO₈ polyhedron has four different A-O bond lengths and different O-A-O angles, as reported in Table 3. Thus, the structure refined with a space group I-4 is much more distorted than the one corresponding to I4₁/a.

3.5. Optical properties

For potential optical applications (luminescence and photo-catalysis), the band-gap energies of the ternary scheelite structure, as well as those of the two binary compounds SrWO₄ and Ce₂(WO₄)₃, were measured by UV-Vis diffuse reflectance spectra DRS at room temperature. This allowed us to discuss the contribution of the insertion of cerium in the scheelite structure. Fig.10 shows the UV-Vis spectra of Sr_{0.50}Ce_{0.35}WO₄, SrWO₄ and Ce₂(WO₄)₃. Large bands were observed for all spectra after 3 eV. According to theoretical calculations reported in the literature, tungstates scheelite materials like SrWO₄ exhibit an optical absorption band due to direct electronic transition (Zhang *et al.*, 1998), which occurs through excitation of electrons from the valence band to the conduction band (Hwang *et al.*, 2003). UV-Vis spectra show that the absorption band obtained for Ce₂(WO₄)₃ is more intense than that of Sr_{0.50}Ce_{0.35}WO₄ and SrWO₄. The intense band observed in the visible region is attributed to the electronic transition of the cerium cation present in the sample.

The energy band gap is obtained by using the Kubelka – Munk method which consists in plotting $F(R_{\infty})$ versus photon energy. The band-gap is deduced by extrapolating the $F(R_{\infty})$ profile using a linear fitting method. R_{∞} designates the reflectance of the sample at infinite thickness and $F(R_{\infty})$ the absolute diffuse reflectance of the sample, which corresponds to the conversion of the reflectance measurements R_{∞} according to the following equation:

$$F(R_{\infty}) = \frac{(1 - R_{\infty})^2}{2R_{\infty}} = \frac{K}{S}$$

where K is the molar absorption coefficient and S the scattering coefficient.

The absorption band gap values for Sr_{0.50}Ce_{0.35}WO₄, SrWO₄ and Ce₂(WO₄)₃ were found to be 3.22, 4.59 and 3.14 eV respectively. The energy gap of the SrWO₄ is well in accordance with the theoretical result of 4,51 eV (Song *et al.*, 2009). In the case of Ce₂(WO₄)₃, the band gap energy of 3,14 eV is in agreement with the one obtained using DFT calculations in a complex

system based on polyoxometalate $[\text{Ce}(\text{W}_5\text{O}_{18})_2]^{8-}$ cluster with CeO_8 polyhedra (Roy *et al.*, 2010). The calculated molecular orbital diagram shows that the electron density consists on the O2p atomic orbital for the HOMO and the Ce 4f orbitals for the LUMO, with a band gap of 3.28 eV. Variations of the gap values can be linked to different factors such as shape and crystallite size (Alivisatos *et al.*, 1996), lattice parameters (Yang *et al.*, 2015), degree of structural disorder in the lattice [Rosa *et al.*, 2008; Lacomba-Perales *et al.*, 2008]. For SrWO_4 , the band gap value shows that the maximum of the valence band can be mainly attributed to O2p levels, while the bottom of the conduction band is mainly composed of W 5d levels. The Sr 5s levels are mainly distributed in the conduction band, thus do not contribute to the band gap. (Song *et al.*, 2009; Arora *et al.*, 2006). The insertion of cerium in the host structure of SrWO_4 can promote different energy distribution at intermediate levels, linked to the 4f, 5d and 6s atomic orbitals, in the band gap near the valence and conduction bands. Combining all these elements, the band structure of $\text{Ce}_{0.35}\text{Sr}_{0.50}\text{WO}_4$ would consist in a valence band with mainly O2p states, and the bottom of the conduction band mainly composed with Ce 4f levels.

To further understand the optical properties evolution of the scheelite structures, the band gap is discussed in terms of microstructural parameters such as bond distance and angles of the polyhedra and the crystallite size.

Generally, it is admitted that the band gap of semiconductors increases when the particle size decreases (Lacomba-Perales *et al.*, 2008). According to a statistical study of grain size distribution based on microscopy images (not reported here), the mean grain size is the same for the different powders, the low band gap value of the ternary compound cannot be attributed to a size effect. Concerning the influence of cell parameters on the band-gap value, the contraction of 1,4% in volume of the cell from SrWO_4 to $\text{Sr}_{1/2}\text{Ce}_{5/14}\square_{1/7}\text{WO}_4$ should induce a small decrease of the band gap (Lacomba-Perales *et al.*, 2008).

According to the data of Table 3, the band-gap decreases with decreasing W-O bond lengths and increasing of A(Sr,Ce)-O bonds lengths. In the same way, all O-W-O and O-A-O angles are much more distorted in the ternary compound refined in the I-4 space group. These changes in bonds and angles correspond to the W-O and A(Sr, Ce)-O stretching and twisting motions. They can be described as a combination of the symmetric and antisymmetric stretches of the oxygen atom bonds in the polyhedra WO_4 and AO_8 . In addition to the vacancies, the presence of cerium ions Ce^{4+} in the structure should induce even more distortions, favouring the appearance of intermediate levels in the band gap. As a consequence, the $\text{Ce}_{0.35}\text{Sr}_{0.50}\text{WO}_4$ scheelite structure gap energy decreases from 4.59 to 3.22 eV, a value very close to those of $\text{Ce}_2(\text{WO}_4)_3$.

4. Conclusion

In the present work, a ternary (Sr,Ce)WO₄ compound has been synthesized using a modified EDTA-Citrate method. The structure was identified as a tetragonal scheelite and the XRD patterns showed well crystallized single phases up to 35%at. of cerium. Electron diffraction and high resolution electron microscopy evidenced the incommensurate modulations linked to partial ordering of Sr²⁺ and Ce³⁺, and the loss of symmetry from the I4_{1/a} space group to the I-4 one. The Rietveld refinement results with the I-4 space group revealed distortions of the AO₈ polyhedra, ie. the local environment of Ce³⁺. The band gap of the ternary compound is significantly lower than the band gap of SrWO₄ and this was related to the 4f atomic orbitals of Ce and the induced crystallographic distortions linked to the incommensurate modulations. The band gap value of 3.2 eV makes Sr_{1/2}Ce_{5/14}□_{1/7}WO₄ a promising candidate for violet luminescence in the 380 nm range.

Acknowledgements - This study was done in the general framework of the french-brazilian cooperation project CAPES COFECUB PHC 77-113.

References

- Abakumov, A.M., Morozov, V.A., Tsirlin, A.A., Verbeeck, J., Hadermann, J., (2014) *Inorg. Chem.*, 53, 9407–9415
- Albino, M., Pechev, S., Veber, P., Velazquez M., Josse, M., (2012) *Acta Cryst.*, C68, i7–i8
- Alivisatos, A. P., (1996) *Science*, 271, 933–937.
- Arab, M., Lopes-Moriyama, A. L., Renovato dos Santos, T., Pereira de Souza, C., Gavarri, J. R., Leroux, Ch. (2013). *Catalysis Today*, 208, 35-41
- Arora, S.K., Chudasama, B., (2006) *Cryst. Res. Technol.*, 41, 1089–1095.
- Cavalcante, L. S., Almeida, M. A. P., W. Avansi Jr., Tranquilin, R. L., Longo, E., Batista, N. C., Mastelaro, V. R., Siu Li, M., (2012) *Inorg. Chem.*, 51 (20), pp 10675–10687
- Culver, S.P., Greaney, M.J., Tinoco, A., Brutchey, R.L., (2015). *Dalton Trans.*, 44, 15042–15048
- Garvie, L.A.J., Buseck, P.R., (1999), *J. Phys. Chem. Sol.*, 60, 1943-1947
- Hwang, D.W., Jae Sung, L., Wei, L., Se Hyuk, O., (2003) *J. Phys. Chem. B.*, 107, 4963-4970
- Jiang, P., Gao, W., Cong, R., Yang, T., (2015). *Dalton Trans.*, 44, 6175-6183
- Lacomba-Perales, R., Ruiz-Fuertes, J., Errandonea, D., Martinez-Garcia, D., Segura, A., (2008) *Europhys. Lett.*, 83, 37002.
- Li, Y. Q., Hirosaki, N., Xie, R. J., Takeda, T., Mitomo, M., (2008), *Chem. Mater.*, 20, 6704-6714
- Longo, V., Orhan, E., Cavalcante, L., Porto, S., Espinosa, J., Varela, J. A., Longo, E., (2007) *Chem. Phys.*, 334, 180.
- Morozov, V.A., Arakcheeva, A.V., Chapuis, G., Guiblin, N., Rossell, M.D., Van Tendeloo, G., (2006). *Chem. Mater.*, 18, 4075-4082

- Morozov, V., Arakcheeva, A., Redkin, B., Sinitsyn, V., Khasanov, S., Kudrenko, E., Raskina, M., Lebedev, O., Van Tendeloo, G., (2012). *Inorg. Chem*, 51, 5313-5324
- Morozov, V., Bertha, A., Meert, K.W., Van Rompaey, S., Batuk, D., Martinez, G.T., Van Aert, S. Smet, P.F., Raskina, M.V., Poelman, D. Abakumov, A.M., Hadermann J., (2013), *Chem. Mat.*, 25, 4387-4395
- Nogueira I.C., Cavalcante L.S., Pereira P.F.S., de Jesus M.M., Rivas mercury J.M., Batista N.C., Siu Li M., Longo E., (2013) *J.Appl.Cryst.*, 46,1434-1446
- Patout, L., Jacob, D., Arab, M., Pereira De Souza, C., Leroux, Ch., (2014). *Acta Cryst B*, 70, 268-274
- Pereira, P.F.S., Nogueira, I.C., Longo, E., Nassar, E.J., Rosa, I.L.V., Cavalcante, L.S., (2015) *J. Rare Earths*, 33, 113-128
- Pinheiro, C.B., Abakumov, A.M., (2015), *IUCRJ*, 2, 137-154
- Rosa, I. L., Marques, A. P. A., Tanaka, M. T., Melo, D. M., Leite, E. R., Longo, E., Varela, J. A., (2008) *J. Fluoresc.*, 18, 239
- Song, M., Zhang, Q., Liu, T., Yin, J., Guo, X., Zhang, H., Wang, X., (2009) *Curr. Appl. Phys*, 9, 812–815.
- Takai, S., Nakanishi, T., Oikawa, K., Torii, S., Hoshikawa, A., Kamiyama, T., Esaka, T., (2004) *Solid State Ionics*, 170,297-304
- Van Smaalen S., *Incommensurate Crystallography*, IUCr Monographs 21, 2007, Oxford Science Publications,
- Volkov, V., Cascales, C., Kling, A., Zaldo, C., (2005), *Chem. Mat.*, 17,291-300
- Yang, X., Fu, Z. Liu, G., Zhang, C., Y. Wei, Wu, Z., Sheng, T., (2015) *RSC Adv.*, 5,70220–70228.
- Zhang, Y., Holzwarth, N., William, R.T., (1998) *Phys. Rev B.*, 57, 12738-12750
- Zhou, Y., He, X.H., Yan, B., (2014). *Opt. Mater.*, 36, 602–607
- Zhu, Q.-Q., Wang, L., Hirosaki, N., Hao, L.Y., Xu, X., Xie, R.-J., (2016) *Chem. Mater.*, 28, 4829– 839

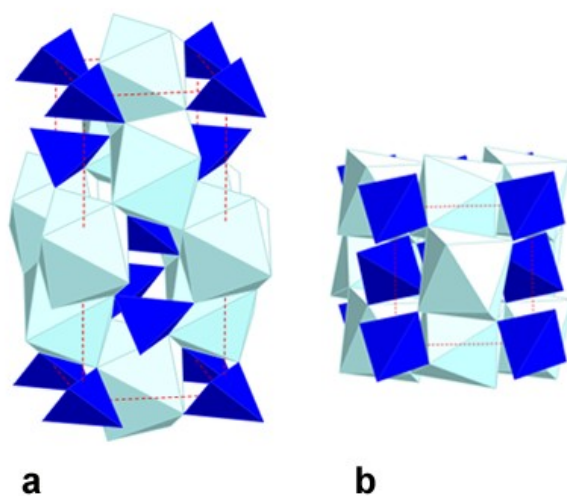


Figure 1 ABO_4 scheelite structure, a) drawing of the unit cell showing the piling up along the c axis of edges-linked AO_8 polyhedra. b) drawing of the unit cell along $[001]$ showing the BO_4 tetrahedra and AO_8 polyhedra are linked by vertices.

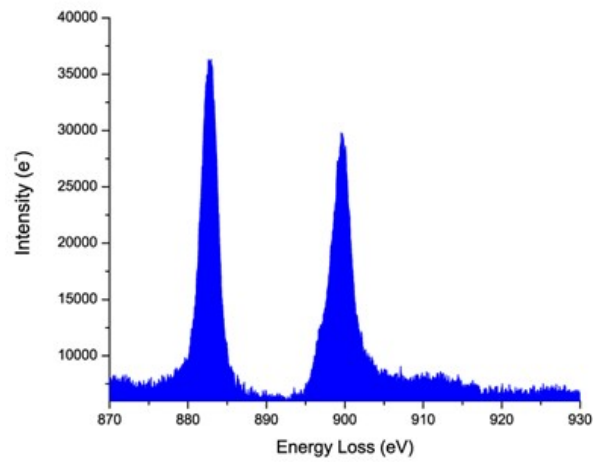


Figure 2 Cerium $M_{4,5}$ core loss edge of $Sr_{0.50}Ce_{0.35}WO_4$.

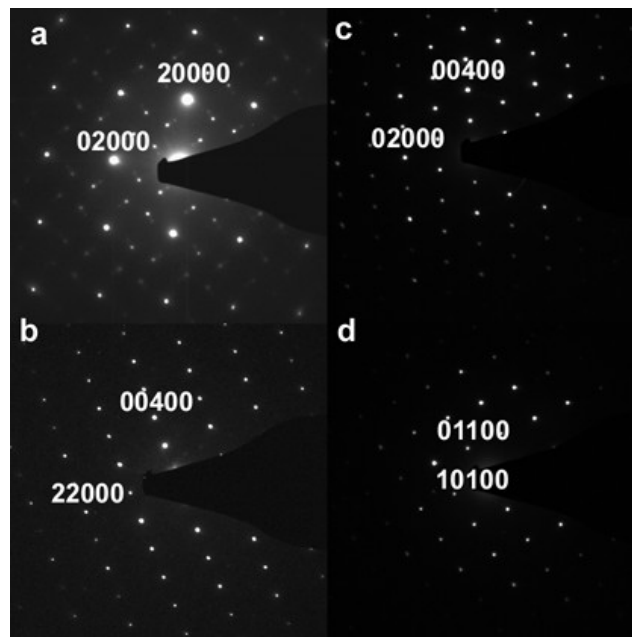


Figure 3 High symmetry electron diffraction patterns of the incommensurately modulated $Sr_{0.50}Ce_{0.35}WO_4$, along the zone axes $[001]$ (a), $[1-10]$ (b), $[100]$ (c), $[11-1]$ (d)

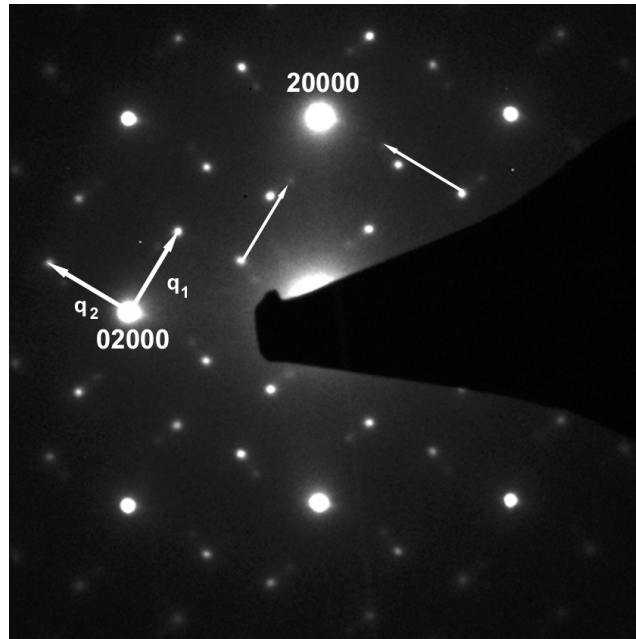


Figure 4 Part of [001] electron diffraction pattern, showing that all supplementary spots are due to the incommensurate vectors q_1 and q_2 .

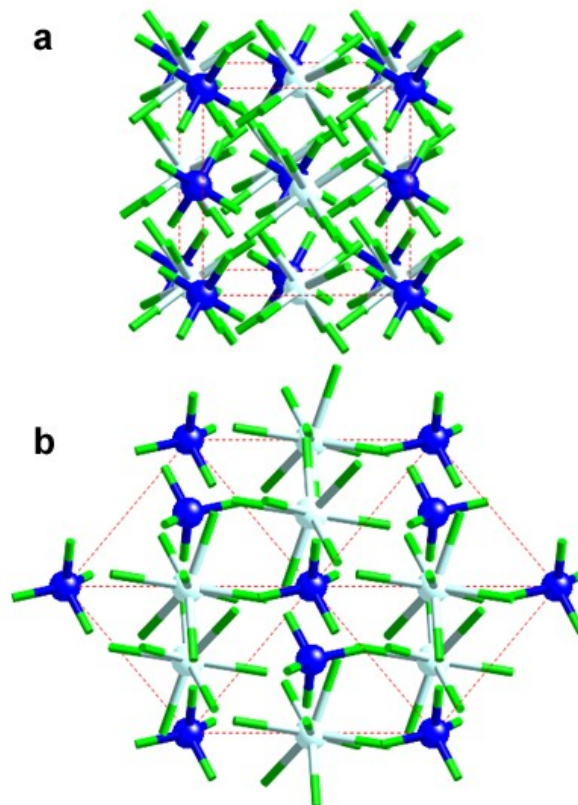


Figure 5 Projection of the ABO_4 structure along two different crystallographic a) $[001]$ and b) $[111]$. A and B cations are drawn as light blue (A) and dark blue (B), and the A-O and B-O links are drawn as sticks.

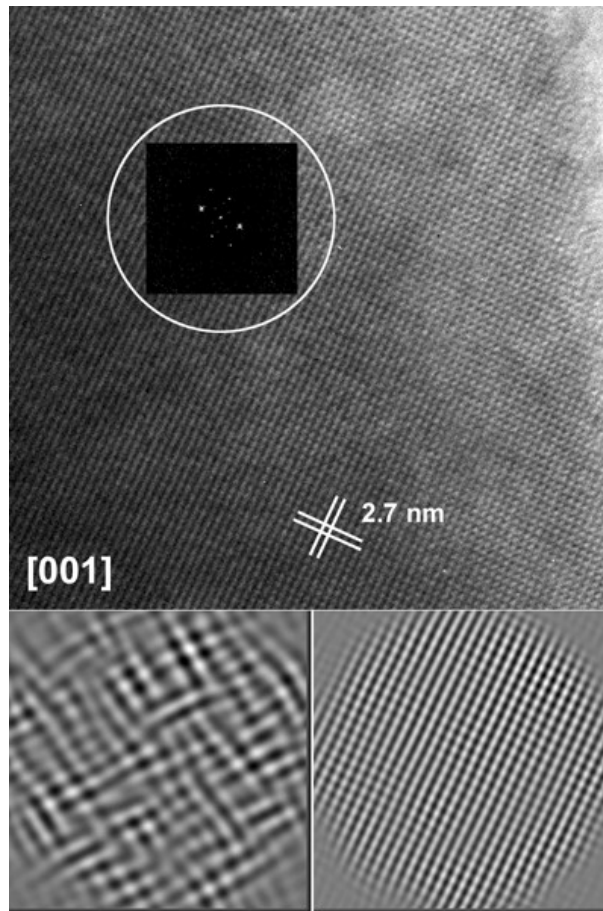


Figure 6 HREM image taken along $[001]$, along with FFT and filtered images.

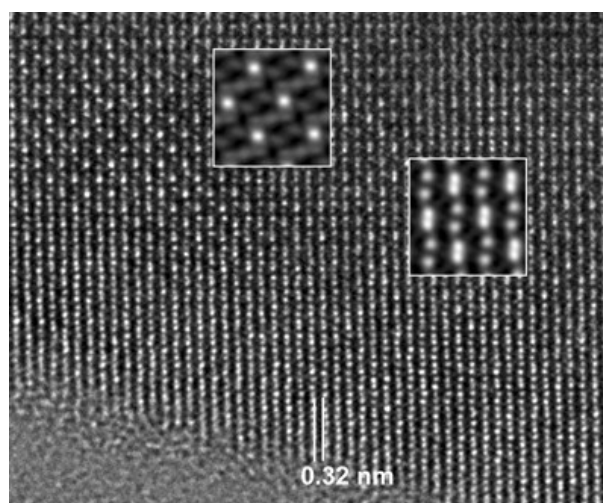


Figure 7 HREM image taken along $[111]$. The inset show two characteristic patterns.

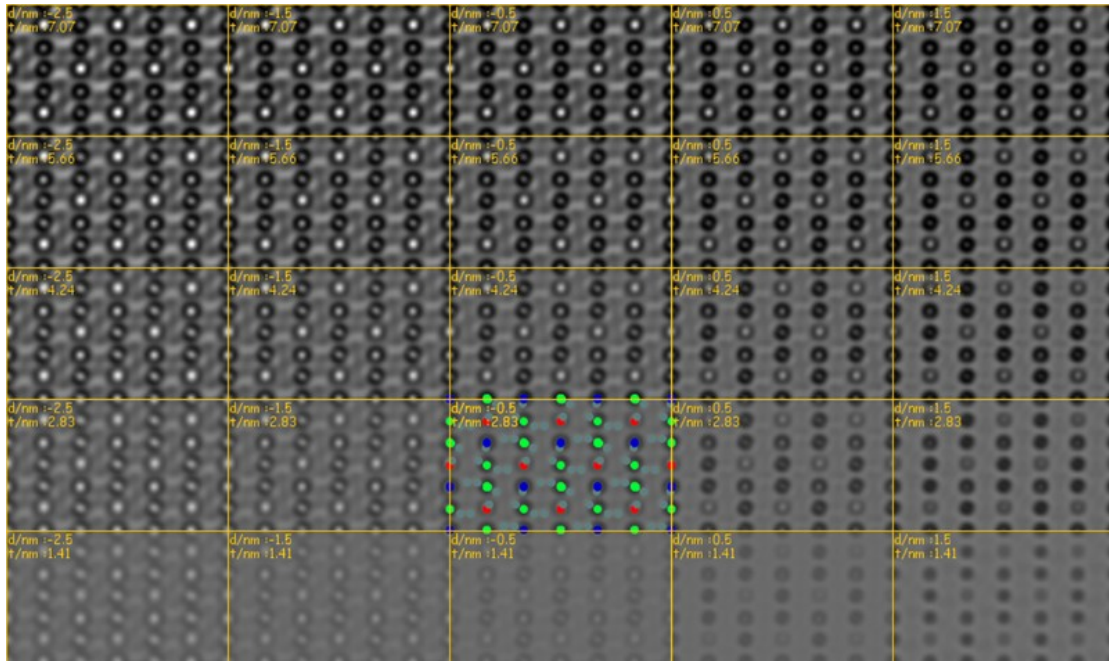


Figure 8 Map of images simulated (model 2). The defocus d varies from 2.5 nm to -1.5 nm, the thickness t from 1.4 nm to 7 nm. Projected atoms are represented as dots, Sr = blue, Ce = red, W = green

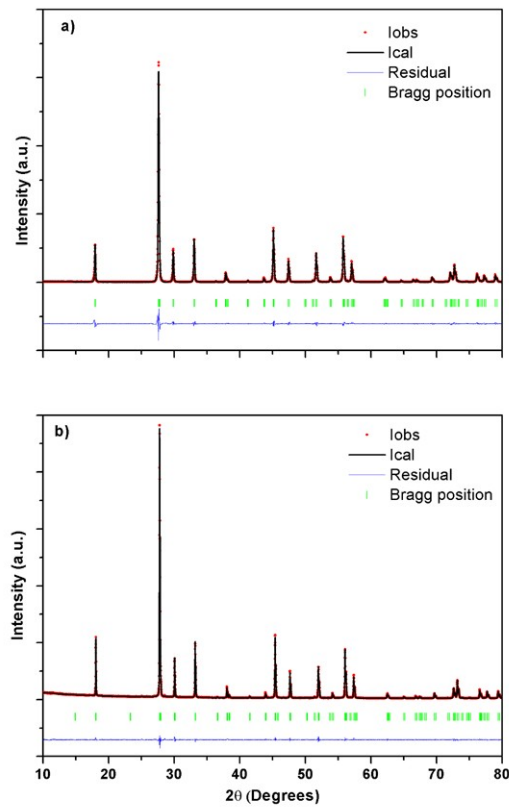


Figure 9 XRD patterns of a) SrWO_4 and b) $\text{Sr}_{0.5}\text{Ce}_{0.35}\text{WO}_4$: observed and refined profiles

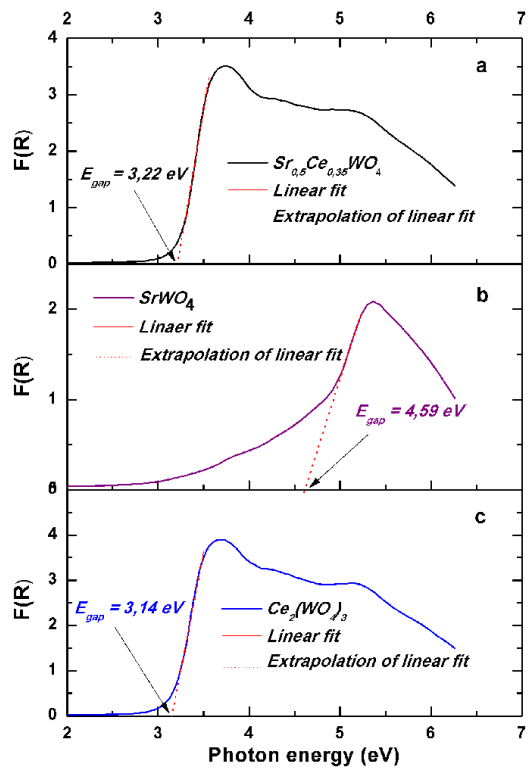


Figure 10 UV-Vis spectra of $\text{Sr}_{0.5}\text{Ce}_{0.35}\text{WO}_4$, SrWO_4 and $\text{Ce}_2(\text{WO}_4)_3$ powders

Table 1 atom coordinates of Sr, Ce, W and O in $I4_1/a$ and $I-4$ space groups

Space group	atome	site	coordinate
$I4_1/a$	Sr,Ce	4b	0,0,1/2 0,1/2,3/4
	W	4a	0,0,0 0,1/2,1/4
	O	16 f	x,y,z
$I-4$	Sr,Ce	2b	0,0,1/2
	Sr,Ce	2c	0,1/2,1/4
	W	2a	0,0,0
	W	2d	0,1/2,3/4
	$\text{O}_1 \text{ O}_2$	8 g	x,y,z

Table 2 Refinement results for the binary SrWO₄ and the ternary Ce_{0.35}Sr_{0.50}WO₄ compounds using two different space groups.

Compound	SrWO ₄	Sr _{0.50} Ce _{0.35} WO ₄	Sr _{0.50} Ce _{0.35} WO ₄	
Space group	I4 ₁ /a	I4 ₁ /a	I-4	
Cell parameters (Å)	a=5.416(8) c=11.975(0)	a=5.394(2) c=11.884(7)	a=5.394(2) c=11.884(7)	
Cell volume (Å ³)	351.363	345.809	345.814	
Oxygen coordinates	O (16f)	O (16f)	O ₁ (8g)	O ₂ (8g)
x	0.2504	0.3559	0.2533	0.6492
y	0.1106	0.0135	0.1395	0.7892
z	0.04121	0.2919	0.9250	0.1601
Reliability factors				
R _p	9.48	6.22	6.68	
R _{wp}	13.4	7.32	7.53	
R _{exp}	7.88	5.07	5.26	
χ ²	2.91	2.08	2.05	
R _{Bragg}	3.59	3.12	2.76	

Table 3

Compound	SrWO ₄	Sr _{0.50} Ce _{0.35} WO ₄	Sr _{0.50} Ce _{0.35} WO ₄		
Space group	I4 ₁ /a	I4 ₁ /a	I-4		
Polyhedra			WO₄		
Bond (Å)	d: W-O	1.840(8)	1.790(4)	1.755(4)	1.796(4)
Angle (°)	O-W-O	106.9	107.7	105.0	104.2
		114.6	113.1	111.7	120.5
				AO₈	
Bond (Å)	A-O ₁	2.533(4)	2.561(4)	2.519(5)	2.581(2)
	A-O ₂	2.571(6)	2.585(0)	2.588(9)	2.675(1)
		68.8	67.9	68.3	65.4
		74.8	73.5	70.2	72.6
		75.6	77.5	79.5	76.8
Angle (°)	O-A-O	76.1	78.5	85.38	77.7
		98.6	98.4	97.2	99.2
		128.3	126.8	122.7	130.5
		134.5	135.1	138.5	132.9
		150.5	151.0	152.8	148.9